A spectroscopic study of trivalent cation (Cm^{3+} and Eu^{3+}) sorption on monoclinic zirconia (ZrO_2)

Eibl, M.; Virtanen, S.; Pischel, F.; Bok, F.; Lönnrot, S.; Shaw, S.; Huittinen, N.;

Originally published:

September 2019

Applied Surface Science 487(2019), 1316-1328

DOI: https://doi.org/10.1016/j.apsusc.2019.05.012

A spectroscopic study of trivalent cation (Cm^{3+} and Eu^{3+}) sorption on monoclinic zirconia (ZrO_2)

Manuel Eibl[1], Sinikka Virtanen[2], Felix Pischel[1,3], Frank Bok[1], Satu Lönnrot[2], Samuel Shaw[4], and Nina Huittinen[1]*

[1)] *Helmholtz-Zentrum Dresden-Rossendorf, Institute of Resource Ecology, Bautzner Landstraße 400, 01328 Dresden, Germany*

[2)] *Department of Chemistry, Radiochemistry, University of Helsinki, P.O. Box 55, 00014 University of Helsinki, Finland*

[3)] *Technische Universität Dresden, Chemie und Lebensmittelchemie, Mommsenstrasse 4, 01069 Dresden, Germany*

[4)] *Research Centre for Radwaste Disposal and Williamson Research Centre, School of Earth, Atmospheric and Environmental Science, University of Manchester, Manchester M13 9PL, UK*

Author email addresses:

m.eibl@hzdr.de, sinikka.m.virtanen@helsinki.fi, felix.pischel@mailbox.tu-dresden.de, f.bok@hzdr.de, satu.lonnrot@helsinki.fi, sam.shaw@manchester.ac.uk, n.huittinen@hzdr.de

*Corresponding author :

Nina Huittinen
email : n.huittinen@hzdr.de
phone : +49 351 260 2148
fax : +49 351 260 3553

Abstract

This study investigates the retention of trivalent actinides (Cm^{3+}) and their lanthanide analogues (Eu^{3+}) on monoclinic zirconia (ZrO_2), a solid phase known to form on the zircaloy cladding material surrounding spent nuclear fuel (SNF) rods. Two zirconia solids with varying carbon content were utilized. The influence of carbon impurities on the ZrO_2 surface charge was investigated via zeta-potential measurements. Batch data was collected for various Eu^{3+} concentrations, while the Cm^{3+} surface speciation was studied on the molecular level with laser spectroscopy (TRLFS). The spectroscopic sorption data was modeled using the Diffuse Double Layer (DDL) model. The ZrO_2 surface charge measurements yielded a pH_{IEP} of 6 which was influenced by the presence of inorganic and organic carbon species. The pH-dependent uptake of Eu^{3+} showed a maximum sorption above pH 5.5, with no impact of the carbon concentration. The speciation of the trivalent metal, however, was different in the presence of intrinsic organic carbon in the sample, resulting in the formation of an organic Cm^{3+}-complex on the surface. This ternary complex was absent on the ZrO_2 material with low carbon content. Here, the surface speciation was dominated by Cm^{3+} and Cm^{3+}-hydrolysis complexes which could be well described by our DDL model.

Keywords: Cm^{3+}, Eu^{3+}, zirconia (ZrO_2), laser spectroscopy (TRLFS), sorption, surface complexation modeling

1. Introduction

Zirconia, ZrO_2, is a frequently studied material from many points of view, one of them being the final disposal of spent nuclear fuel (SNF). In this context, zirconia will be present as a corrosion product of nuclear fuel rod zircaloy cladding used in water cooled reactors. The use of zircaloy as cladding material has been developed since the early 1950s and has experienced several advances since then. Although zircaloy is a collective term for many different alloy compositions they all share a very high zirconium content of above 95%.[1] This alloy has very good characteristics regarding the low thermal neutron capture cross-section as well as high corrosion stability in contact with water at elevated temperatures. Nevertheless, it has been shown that corrosion of the alloy, producing mainly ZrO_2, occurs during reactor operation, and is likely to proceed in a final repository for nuclear waste.[2] A key topic of research in the field of final repository safety is the investigation of immobilizing interactions, such as sorption and incorporation, between solid surfaces present in such a repository, and actinides (e.g. Np, Pu, Am) which are considered the most ecologically and toxicologically problematic contents of SNF after about 100 years after removal from the reactor core, when the short-lived fission products have mostly decayed. Many studies can be found for the interaction of actinides with various clay minerals in host rock formations [3–10] or in envisioned buffer and back-fill materials [11–26]. In addition several studies report on actinide sorption reactions with crystalline (host) rock [27–30], various iron minerals as corrosion products from SNF steel canisters [31–35] and aluminium-bearing solids as representatives for aluminosilicates [36–40] or iron containing solid phases [31,41–44]. However, the interaction of radionuclides, especially the actinides, with the zirconia surface in aqueous systems has received very little attention. Some studies have been performed on the sorption of U(VI) on zirconia [45–47] while only two studies can be found on the sorption of trans-uranium elements, i.e. Pu(IV) [48] and Pu(IV) and Np(V) [49]. To our knowledge no studies can be found on the sorption of trivalent actinides on zirconia, even though these actinides are of great importance for the safety case of final waste repositories, as two Am(III)-isotopes (Am-243 and Am-231) as well as Pu(III) (mainly Pu-239) are the dominating sources of the long-term radiotoxicity in SNF.[50] After water ingress to a final repository, meaning that water has made its way through the geological barrier (the host rock), the geotechnical barrier (the backfill) and the technical barrier (the SNF container), the corrosion of the zircaloy cladding will lead to the formation of zirconia in direct contact with dissolved elements from the SNF matrix. The contact of water with the fuel can lead to oxidative dissolution of the matrix followed by mobilization of radionuclides including the

actinides. Therefore, interactions of actinides with zirconia are highly relevant for analyzing the risk of actinide mobilization in a repository system.

Zirconia is a very complex material with several different crystalline polymorphs with monoclinic, orthorhombic, tetragonal, and cubic crystal systems, which are stable at different pressures and temperatures. The tetragonal and the cubic structures are present at high temperatures, i.e. above 1170 °C and 2370 °C [51], respectively, while the orthorhombic structure is formed at high pressure. Therefore, the monoclinic phase of zirconia is thermodynamically the most stable phase at conditions present in a radioactive waste repository. In addition, the surface properties of zirconia are very diverse, which is apparent when looking at e.g. published data for the isoelectric point of the zirconia surface, for which values ranging from 4 to 10, have been reported.[52]

Zirconia has been claimed to be the only metal oxide with a surface showing acidic and alkaline as well as oxidizing and reducing properties.[53] The alkaline properties of the surface lead to the formation of stable carbonate species on zirconia, which form either from the adsorption of CO_2 from air or due to the dissolution of CO_2 in aqueous solutions.[54] In addition, the crystal structure has been shown to influence the coordination of sorbents on the surface, where especially bicarbonates as well as monodentate and bidentate carbonate species have been observed at the surface of monoclinic zirconia. Besides carbonate species, also organic compounds have a high tendency to chemically sorb on the material as has been shown for pyridine or diphenylamine for example.[53] Commercial production paths of zirconia often involve organic surfactants to improve its properties in different ways. Various different surfactants are used, ranging from fatty acid esters, phenyl ethers to polymers of carboxylic acids.[55] How the presence of such organic compounds or chemisorbed carbonate complexes influences the surface properties of zirconia is not well understood and, hence the effect on the surfaces behavior is often neglected. Therefore it is of great importance to minimize the amount of any remaining surfactant when performing surface investigations to be able to achieve reproducible results as well as to gain knowledge relevant to the safety case of a final SNF repository.

The aim of this study is to investigate the uptake of trivalent cations (Cm^{3+} and Eu^{3+}) on monoclinic zirconia. Comparative adsorption investigations on a commercial, untreated zirconia and the same solid phase after heat-treatment at 1000 °C have been done to study the influence of organic and inorganic impurities on zirconia on the surface properties of the mineral as well as on the surface complexation reaction. The mineral properties before and

after calcination have been studied by means of x-ray diffraction, dissolved organic and inorganic carbon measurements, zeta potential measurements, and scanning electron microscopy. The surface sorption behavior of the trivalent metal cations has been investigated in batch-sorption investigations using Eu^{3+}, while the speciation was studied with time-resolved laser-fluorescence spectroscopy (TRLFS) of Cm^{3+}. To support our findings, surface complexation modelling was performed to create a sorption model for Cm^{3+} on ZrO_2, based on the spectroscopically determined surface speciation. The Diffuse Double Layer model was used to describe the system.

2. Materials and methods

Two ZrO_2 materials were used in this study, differing in their pre-treatment procedures only. One solid has been used as received from ChemPUR without any further treatments, in the following referred to as ZrO_2-untreated. The other has been heat-treated by means of calcination for 5 h at 1000 °C under ambient atmosphere in a ceramic crucible (ZrO_2-calc.). A heating rate of 200 °C/h was used. After the completed calcination time, the oven was switched off and left to cool. The calcined product was ground using an agate mortar and pestle. Both solid phases were subjected to the same characterization methods as described below.

2.1. ZrO_2 characterization methods

The phase purity and crystallinity of the untreated and calcined solids were determined by powder x-ray diffraction (PXRD) using a MiniFlex 600 (Rigaku) diffractometer. For detailed measuring conditions see the supplementary information (SI). To obtain information on the phase composition the Rietveld method was brought to use by using the PDXL software (version 2) from Rigaku.

For the determination of the reflex half-widths (full width at half maximum, FWHM) the average FWHM of the two most intense reflexes at positions of 28.2 ° $(11\bar{1})_m$ and 31.5 ° $(111)_m$ was used. The FWHM is mainly dependent on two parameters being the crystallite size and the crystallinity. Small crystallites will yield broader peaks than larger crystallites, while an increasing crystallinity of the sample will result in narrower diffraction patterns. Therefore, the *Scherrer* equation [56] can be used to calculate the crystallite size from the PXRD pattern, see SI, equation SI1.

The average crystallite sizes D_{hkl} obtained for the two most intense reflections (see above) was used. For further information the reader is referred to the SI.

The specific surface area of the zirconia powder was investigated using N_2-BET physisorption method. These studies were done using a Micromeritics Gemini V, model 2365. Further details are given in the SI.

The morphology and particle size as of the zirconia particles was investigated with SEM. For the SEM investigations, a Quanta 650 SEM of the company ThermoFisher Scientific was used.

Total carbon (TC), total organic carbon (TOC), and total inorganic carbon (TIC) determinations of the solid phases were performed with a COULTER SA 3100 of the Beckman company. The TIC was calculated from the measured TC and TOC concentrations. For a detailed description the reader is referred to the SI.

To investigate the surface properties of the samples and the possible influence of organic and inorganic carbon impurities in the ZrO_2 solids on their electrophoretic behavior, zeta-potential measurements were conducted using untreated and calcined zirconia with a Zetasizer Nano (Malvern Panalytical). Due to the surface basicity of ZrO_2, carbon dioxide has a tendency to adsorb on the solid, which alters the surface charge of the mineral. Thus, zeta-potential measurements of both solids were conducted in the absence and presence of atmospheric CO_2. The sample rows were prepared using a mineral concentration of 1 g/L for ZrO_2-untreated and 0.5 g/L for ZrO_2-calc because of its lower suspension stability. For all samples 10 mM $NaClO_4$ was used as electrolyte. All measurements were done after three days equilibration of the suspensions.

2.2. Eu^{3+} Batch sorption experiments on ZrO_2

Batch sorption experiments, examining the sorption of Eu^{3+} on both zirconia materials as a function of pH were performed. All samples and reagents were prepared in a glove box under nitrogen atmosphere (O_2 < 1 ppm) to exclude any influence from atmospheric CO_2. Carbonate free MilliQ water was used in the preparation of all solutions. 10 mM $NaClO_4$ was used as background electrolyte. Several different Eu^{3+} concentrations in the range from $1 \cdot 10^{-7}$ M to $1 \cdot 10^{-5}$ M were used and the solid concentrations were varied from 0.5 g/L – 5.0 g/L. A detailed summary of the experimental conditions used in these investigations is given in Table S1.

The samples were shaken for a minimum period of three days. Samples were separated by centrifugation with a relative centrifugal force of 4025 *g* for one hour. The Eu^{3+} concentration in the supernatant was measured with inductively coupled plasma-mass spectrometry (ICP-MS).

2.3. TRLFS studies of the Cm^{3+} surface complexation on ZrO_2

The spectroscopic investigations of the Cm^{3+} surface complexation and *in-situ* speciation were done at a Cm^{3+} concentration of $5 \cdot 10^{-7}$ M and a solid concentration of 0.5 g/L in all samples if not specified differently.

TRLFS was utilized to obtain luminescence emission spectra which gives information on changes in the first coordination sphere of Cm^{3+}. The luminescence lifetime measurements yield information on the number of luminescence quenching entities, mainly OH^- and H_2O, in the first coordination sphere of Cm^{3+}. This is done by correlating the measured luminescence lifetime (τ) with the number of hydration water molecules using the semi-empirical *Kimura* equation [57] (Equation 1):

$$N_{H_2O} = \frac{0.65}{\tau_{Cm^{3+}}(ms)} - 0.88 \qquad (1)$$

The pH dependent sorption and speciation of Cm^{3+} on ZrO_2 was investigated with parallel samples containing Cm^{3+}, ZrO_2 and 10 mM $NaClO_4$ as electrolyte. The pH of the samples was increased stepwise from pH 3 to pH 12. After each pH adjustment the samples were equilibrated for two days while constantly stirred. For the TRLFS measurements the samples were pipetted into cuvettes which were sealed in the glove box. After the measurements, the samples were brought back into the glove box and pipetted back to the sample vials, followed by pH adjustments of the complete sample volume.

The TRLFS sorption analyses were performed using a pulsed dye-laser (NarrowScan, Radiant Dyes) with a 1:1 dye mixture of Exalite 389 and Exalite 398, coupled to a Nd:YAG (Continuum, Surelite) pump laser. The Cm^{3+} luminescence emission spectra were recorded between 570 - 640 nm, 1 µs after the exciting laser pulse with a wavelength of 396.6 nm. The laser pulse energy was measured by a pyroelectric energy sensor and was found to be between 2 – 3 mJ in each measurement. Luminescence emission was detected by an optical multichannel analyzer (Shamrock 303i) with 300, 600 or 1200 lines/mm grating and an ICCD-Camera (iStar, Andor). Lifetime measurements were performed by monitoring the luminescence emissions with 5 µs – 20 µs time delay steps between the laser pulse and the camera gating.

2.4. Surface complexation modelling

To create a model based on a chemically realistic surface speciation, the calculated species distribution on the calcined material ZrO_2-calc was used to fit the formation constants (log$K$°) for the three different surface species, obtained from TRLFS (see sections 3.2 and 4). The number of water molecules in the coordination sphere of the proposed species have been calculated from the recorded luminescence lifetime data using the *Kimura* equation (see sections 2.3 and 3.2). The deprotonation of the surface hydroxyl-entities upon Cm^{3+} sorption on the ZrO_2 surface was tested for various degrees of deprotonation (dissociation of only one hydroxyl-entity upon full dissociation of all participating surface OH-groups). The reactions described below showed the best fits and were therefore used in the final calculations.

Species 1: $2\ ZrOH + Cm^{3+} + 7\ H_2O \rightarrow (ZrO)_2Cm(H_2O)_7^{+} + 2\ H^{+}$

Species 2: $3\ ZrOH + Cm^{3+} + 6\ H_2O \rightarrow (ZrO)_3Cm(H_2O)_6^{\pm 0} + 3\ H^{+}$

Species 3: $5\ ZrOH + Cm^{3+} + 4\ H_2O \rightarrow (ZrO)_5Cm(H_2O)_4^{2-} + 5\ H^{+}$

The surface site density (SSD) of ZrO_2 was calculated using a crystallographic approach. The morphology of ZrO_2 crystals was calculated with the BFDH (Bravais-Friedel-Donnay-Harker) model using the software package "Mercury CSD 3.9" [58] and the crystallographic data from Smith and Newkirk [59]. For each surface plane, the number of oxygen atoms per square-nanometer was determined assuming that each surface oxygen atom is equivalent to one hydroxylic group that is capable for metal-ion binding reactions. Only the oxygen atoms of the Zr-O-octahedron corners in the uppermost layer were considered, since these are directly accessible for a sorption reaction. For the overall SSD value, the mean SSD value of all planes was calculated and weighted by the relative BFDH area of each plane. For the surface protolysis reactions, the data from Blackwell and Carr [60] was used. For the fitting procedure the parameter estimation software 'UCODE2014' [61] was coupled with the geochemical speciation code 'PHREEQC' [62] using the aqueous speciation and mineral solubility data based on the 'PSI/Nagra Chemical Thermodynamic Database 12/7' [63].

3. Results

3.1. Mineral characterization

Both used materials, the untreated (ZrO_2-untreated) and the pretreated (ZrO_2-calc), show the diffraction pattern of the monoclinic phase (Figure 1). However, the untreated material additionally shows a small percentage (~ 4%) of the tetragonal phase. The ZrO_2-untreated shows narrow diffraction peaks (FWHM ~ 0.49 °), which decrease in half-width after heat treatment to approximately 0.19 °. Using the *Scherrer* equation (equation SI1) the crystallite size of ZrO_2-untreated could be calculated (see explanations in section 2.1. and SI) to be around 20 – 25 nm which correlates well with the size of 20 nm given by the producer. In contrast, the heat treated product has a calculated crystallite size of approximately 45 nm assuming a constant crystallinity.

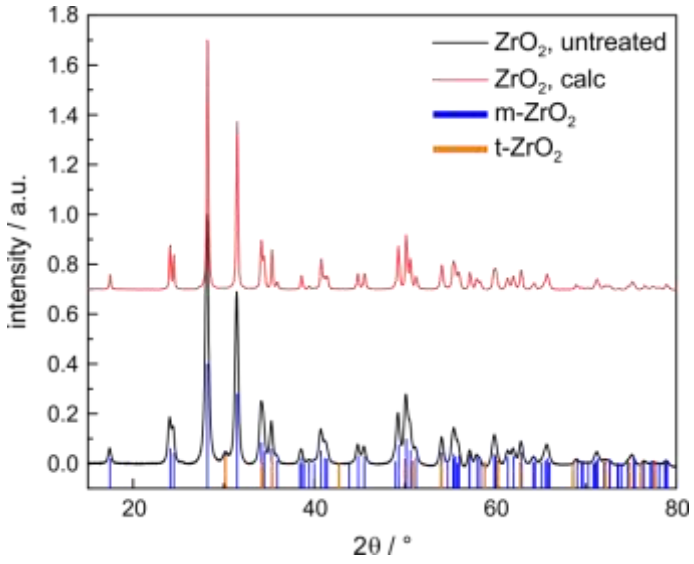

Figure 1: X-ray diffraction pattern of the untreated (ZrO_2-untreated) and the calcined material (ZrO_2-calc) using Cu-Kα radiation. The reflexes of the monoclinic and the tetragonal phases of ZrO_2 are indicated with bars in the figure.

The particle size distribution of ZrO_2-untreated (Figure 2, left) and ZrO_2-calc (Figure 2, right) gives a size of 135 ± 27 nm and 96 ± 32 nm, respectively. This implies that the particle size of the calcined material subjected to both calcination and grinding is similar to the original product (Figure 2, top). The particle size differs strongly from the crystallite size, therefore, the observed particles consist of multiple crystallites.

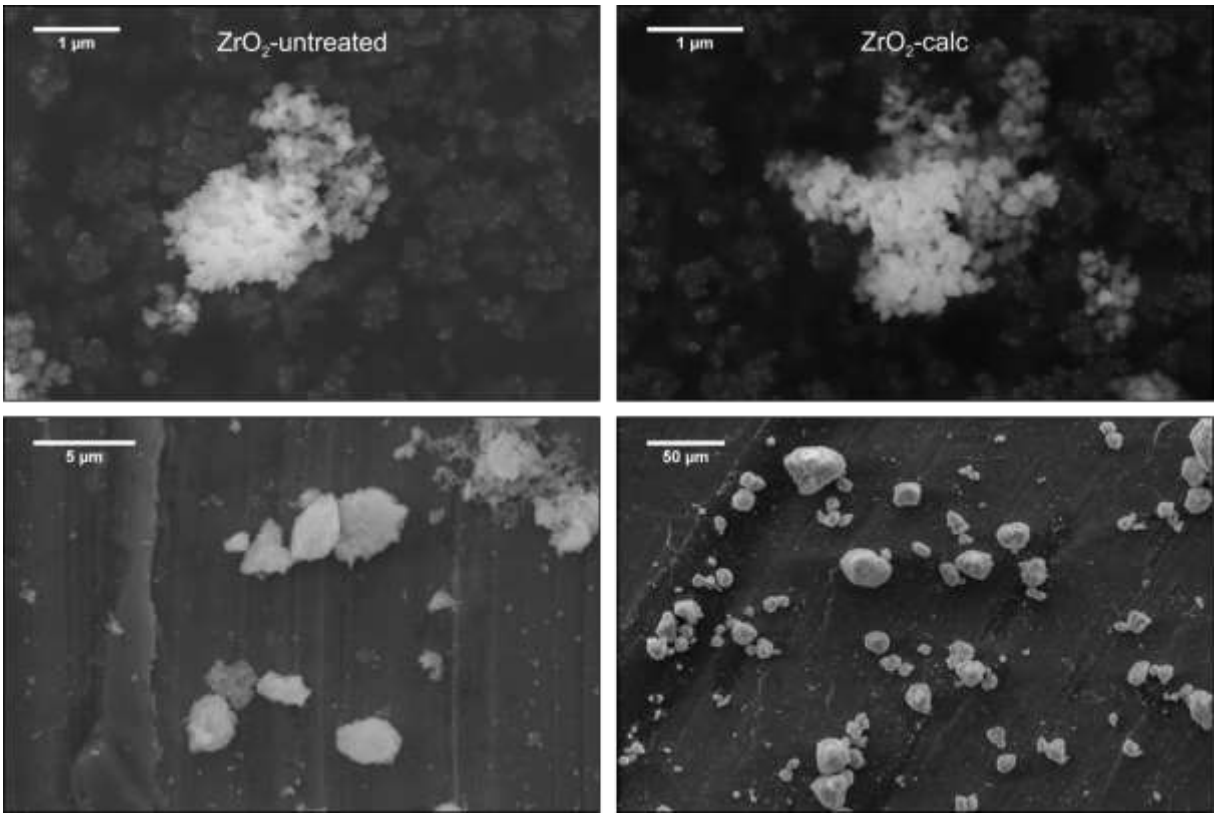

Figure 2: ZrO_2-untreated, applied to the sample holder as powder (top left) and from suspension (bottom left), ZrO_2-calc, applied to the sample holder as powder (top right) and from suspension (bottom right).

In Figure 2, bottom, the agglomerate size of both samples is shown when applied to the sample holder from aqueous suspension. Although the particle size was shown to be very similar, the size of the agglomerates of ZrO_2-untreated is smaller, i.e. 3 ± 2 µm compared to 13 ± 6 µm for ZrO_2-calc which manifests in its higher suspension stability.

The BET surface area of the commercial material (ZrO_2-untreated) is 21.8 ± 0.2 m^2/g while the area of the calcined and mortared material (ZrO_2-calc) is considerably smaller with a value of 5.6 ± 0.1 m^2/g. The micro pore area for both materials is 1.26 ± 0.02 m^2/g.

The ZrO_2-untreated shows a total carbon content of 0.98 ± 0.06 mg/g while the distribution of organic to inorganic carbon is about 50% each (Table 1). Upon calcination of the ZrO_2-untreated the carbon content decreases drastically to 0.13 ± 0.03 mg/g, most likely due to the combustion of an organic carbon source initially present in the sample as well as the removal of carbonate species from the surface. Here, the detection limit does not allow any distinguishing between organic and inorganic carbon. However, due to the high calcination temperature it can be assumed that all carbon sources initially present on the surface have been removed and it seems reasonable to assume that the remaining carbon is re-adsorbed CO_2 and therefore inorganic carbon from air.[64–66]

Table 1: Measured total carbon (TC), total organic (TOC) and total inorganic carbon (TIC) concentrations in the zirconia phases.

	TC [mg/g]	TOC [mg/g]	TIC [mg/g]
ZrO_2-untreated	0.98 ± 0.06	0.48 ± 0.03	0.50 ± 0.03
ZrO_2-calc	0.13 ± 0.03	-	-

In the presence of CO_2, both solids show very similar surface charge behavior as a function of pH in 10 mM $NaClO_4$ (Figure 3, open symbols). An isoelectric point (IEP) between pH 6.8-7.3 can be determined but no apparent correlation between the IEP and the TC can be found.

The pH dependent zeta-potential curves at inert conditions of ZrO_2-untreated (Figure 3, top, filled symbols) and ZrO_2-calc (Figure 3, bottom, filled symbols), however, differ strongly from each other. The IEP of the ZrO_2-untreated is found to be 9 while ZrO_2-calc has an IEP of 5.8. This clear difference in the IEP in dependence of the pre-treatment method is a strong indication for a surface contamination initially present before the heat-treatment.

The zeta-potential of the ZrO_2-calc shows strongly scattered values. This is because of bad suspension stability, as observed during the experiments, which is caused by the high agglomeration tendency of the treated material, although a lower solid to liquid ratio (0.5 g/l instead of 1.0 g/l) was used.

At inert conditions the IEP of both materials differs strongly from each other, however, at ambient conditions the IEP is nearly identical. Therefore it can be assumed that the influence of CO_2 on the surface charge exceeds the effect of the presumed organic contamination. However, as the batch sorption and spectroscopic investigations in the present study were conducted in the absence of CO_2, the different surface charge properties of the two sorbents may have an influence on the uptake and speciation of the trivalent metal cations on the two zirconia materials. To compare the behavior in the absence and presence of atmospheric CO_2 the zeta-potential curves of both materials are replotted for inert conditions and for ambient conditions in Figure S1.

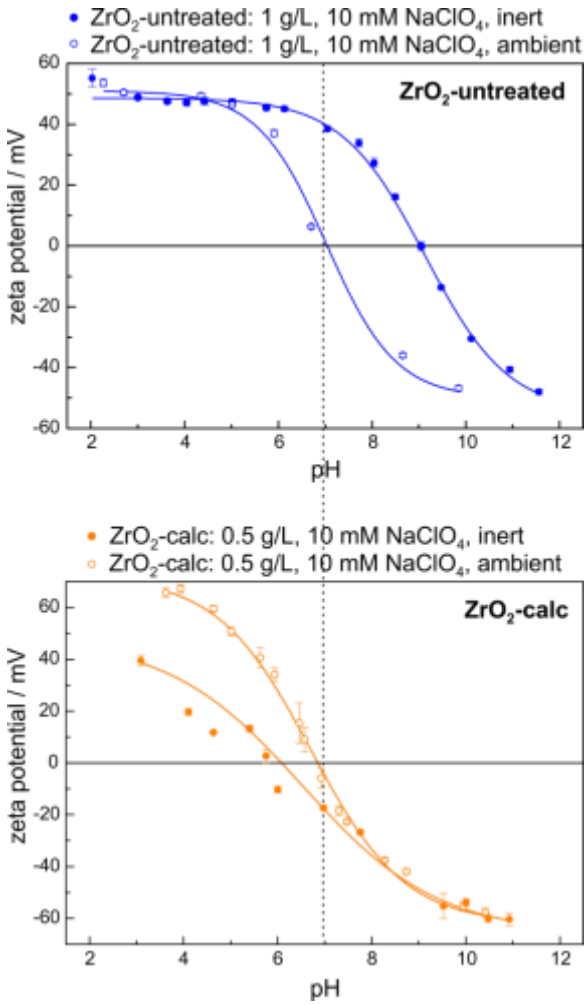

Figure 3: Zeta-potential as a function of pH for untreated (top) and calcined (bottom) zirconia prepared in a CO_2-free glove box (filled symbols) and after exposure to the atmosphere (open symbols). The black dotted line is added to visualize the very similar pH_{IEP} of both materials at ambient conditions and the strongly differing pH_{IEP} at inert conditions.

3.1.1. Eu^{3+} Batch-sorption experiments on ZrO_2

The batch-sorption curves of ZrO_2-untreated at various conditions ranging from $1 \cdot 10^{-7}$ M Eu^{3+} on 5 g/L up to $6 \cdot 10^{-6}$ M on 2 g/L, which corresponds to a range from $2 \cdot 10^{-8}$ mol/g to $3 \cdot 10^{-6}$ mol/g, show a very similar curve shape in Figure 4, left. Only at a concentration of $1 \cdot 10^{-5}$ M on 0.5 g/L ($2 \cdot 10^{-5}$ mol/g) a shift of the sorption edge can be observed, which could be the result of reaching a high surface coverage. Therefore, it can be assumed that at concentrations higher than $3 \cdot 10^{-6}$ mol/g different sorption sites (strong vs. weak sites), repulsion between already adsorbed Eu^{3+} and Eu^{3+} ions in solution, or steric effects on the surface, influence the sorption reaction. The sorption curve of the pre-treated material shows a very similar curve shape when a low metal to solid ratio of $2 \cdot 10^{-7}$ mol/g ($1 \cdot 10^{-7}$ M on 0.5 g/L)

is used (Figure 4, right). However, a slight shift of the sorption curve becomes apparent at a Eu^{3+} concentration of $6 \cdot 10^{-6}$ M on 2 g/L ZrO_2-calc ($3 \cdot 10^{-6}$ mol/g).

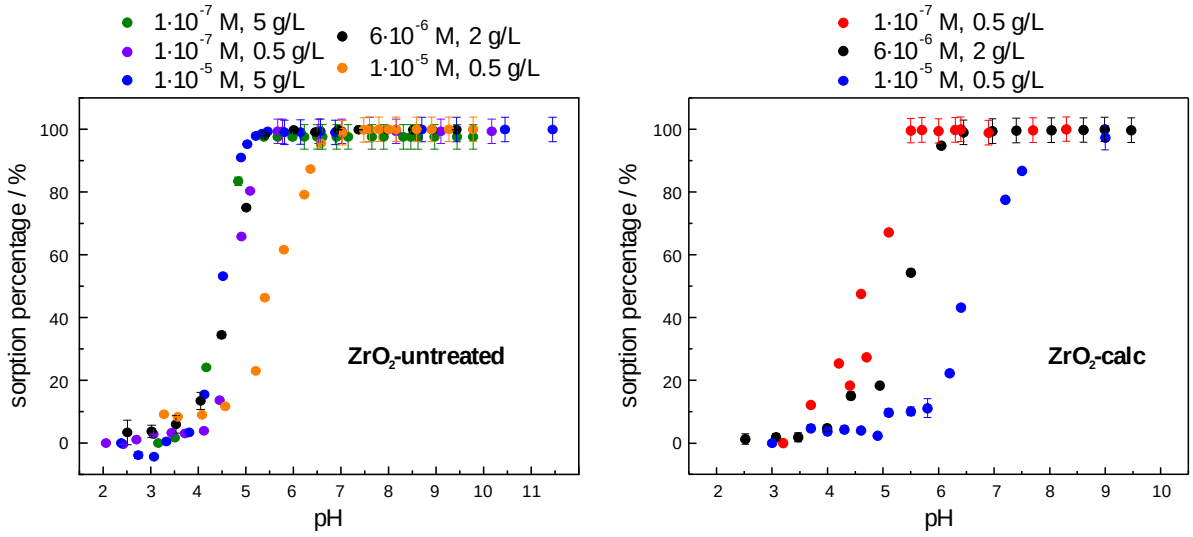

Figure 4: Eu^{3+} batch-sorption curves of ZrO_2-untreated (left) and ZrO_2-calc (right) in varying metal to mineral ratios with 10 mM $NaClO_4$ background electrolyte.

The reason for the higher sorption capacity of the untreated material could be due to various reasons. The largest influence, however, will be the surface area, which is almost four times higher for the untreated material (21.8 ± 0.2 m^2/g) compared to the calcined one (5.6 ± 0.1 m^2/g), as the surface area for a given amount of solid correlates with the absolute amount of surface sites. Thus, to allow for better comparison of the batch sorption curves, obtained Eu^{3+} sorption distribution coefficients were normalized with respect to the specific surface area of the ZrO_2 materials and selected curves with relevant metal to solid ratios were compared (Figure S2).

The edge position remains rather constant for the batch sorption curves in the relevant concentration range, implying that the observed differences in the percentage of adsorbed Eu^{3+} on the two different zirconia materials can be attributed to differences in the specific surface area and that maximum sorption occurs from a pH of about 5.5. Some minor differences can be seen for the sorption curve of $1 \cdot 10^{-7}$ M on ZrO_2-calc. This may be an effect of experimental error only, however, the lower IEP measured for the calcined material and consequently the predominance of negatively charged surface groups above pH 6 could enhance the sorption of positively charged cations in comparison to the untreated material with a very high IEP (pH_{IEP} = 9). Surface saturation can be excluded as the reason for the small shift as the surface coverage for the sorption of $6 \cdot 10^{-6}$ M Eu^{3+} on 2 g/L ZrO_2-calc can be

calculated to be 19% at a surface site density of 7.56 sites/nm^2. This site density was obtained by calculations based on the BFDH model (as explained in 2.4).

3.2. TRLFS studies of the Cm^{3+} surface complexation on ZrO_2

Recorded emission spectra for Cm^{3+} sorption on untreated and calcined ZrO_2 are presented in Figure 5. For the calcined product, the emission spectra show a continuous bathochromic shift as a function of pH, a behavior which is typically noted for the pH-dependent sorption of Cm^{3+} on various mineral surfaces (see e.g. references given in Table 2).

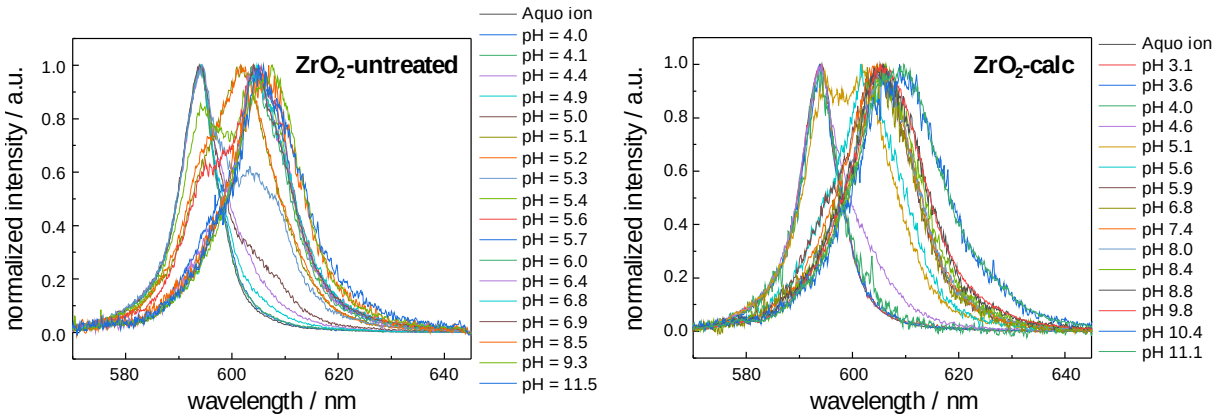

Figure 5: Emission spectra of $5 \cdot 10^{-7}$ M Cm^{3+} on 0.5 g/L ZrO_2-untreated (left) and on 0.5 g/L ZrO_2-calc (right) in dependence of the suspension pH (λ_{ex} = 396.6 nm).

The situation is different for the untreated product, where a red-shifted shoulder appears in the mildly acidic pH-range. This is visualized in Figure 6 for two different sets of samples.

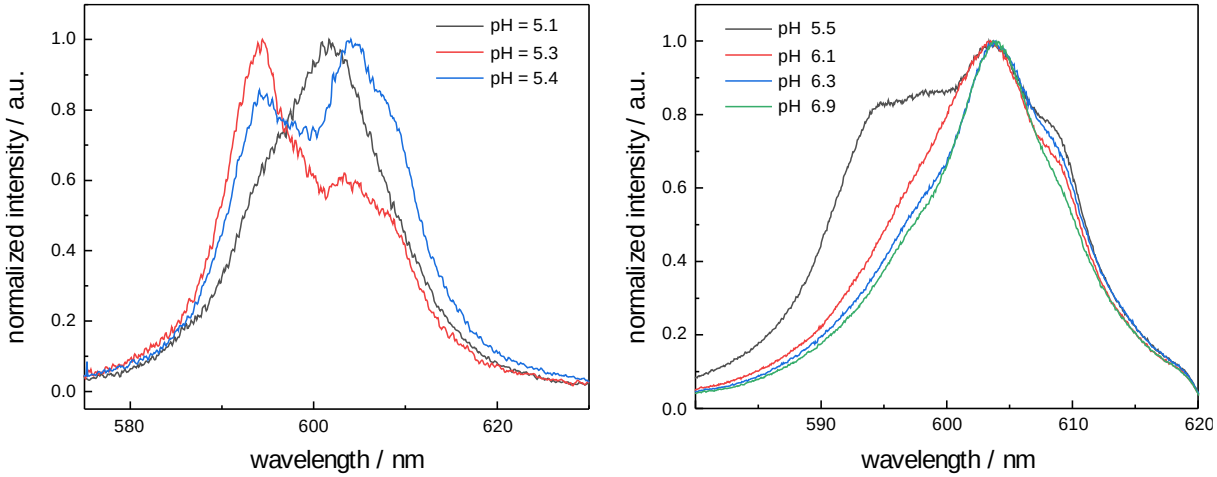

Figure 6: Selected emission spectra of $5 \cdot 10^{-7}$ M (left) and $1 \cdot 10^{-7}$ M of Cm^{3+} (right) sorbed onto ZrO_2-untreated (λ_{ex} = 396.6 nm), both showing unexpected peak shift behavior.

On the left in Figure 6, the emission spectra in the pH region from 5.1 to 5.4 are presented, showing a strong shift first to lower, then to higher wavelengths despite of relatively small pH

changes. The emission spectra are taken from three different samples, prepared in parallel under constant conditions. Since all samples were prepared from the same mineral and Cm^{3+} stock solutions, significant variations in their concentrations are not to be expected. In Figure 6, right, a clearly visible shoulder appears from a pH of 5.5. Here, two samples have been used at pH 5.5 and 6.3 and the pH of these samples has been raised to 6.1 and 6.9, respectively. The observed differences in the spectra can be interpreted as a blue shift with increasing pH which cannot be explained in a pure two component sorption system. Within this pH region the shoulder is at times more, at times less pronounced in a non-systematic manner. These observations make it very clear that another component is taking part in the sorption process altering the sorption behavior of curium at the zirconia surface.

To obtain single component spectra from the emission spectra, we performed a species deconvolution. For that, a subtraction of the emission spectrum of the aquo ion is performed from the spectrum where the first species differing from the aquo ion is observed. By this procedure, a pure spectrum of the first species, species 1, can be obtained. This spectrum can thereafter be used together with the spectrum of the aquo ion to extract the next species, appearing at increasing pH. For a more detailed description of this process, the reader is referred to the SI.

The extraction of single component spectra from this set of data is difficult, due to the incongruent spectral evolution as a function of pH. Several species are present simultaneously in the suspension, and a situation where only one sorbed species on the zirconia surface is present at a time in addition to the aquo ion in solution, hardly exists. Nevertheless, a tentative deconvolution was performed, resulting in four single component spectra for sorbed Cm^{3+}-species with emission peak maxima at 600.4, 604.1, 608.8 and 613.3 nm (Figure 7, left).

The extraction of pure components for Cm^{3+} sorption onto the calcined material from the pH dependent emission spectra yielded three pure component spectra with peak positions at 602.3, 606.2 and 612.5 nm, Figure 7, right. The peak positions clearly differ from the species observed on the pristine material and are extremely red-shifted when comparing to peak positions observed for Cm^{3+} adsorbed on other mineral phases, see Table 2.

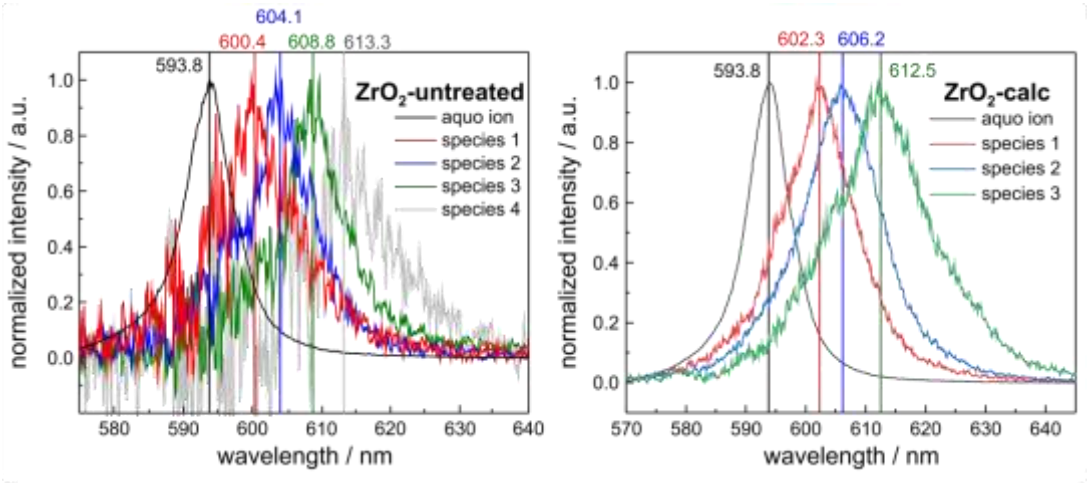

Figure 7: Deconvoluted single species emission spectra for the sorption of Cm^{3+} on ZrO_2-untreated (left) and of ZrO_2-calc (right).

Table 2: Comparison of the emission maxima of Cm^{3+} sorption species on zirconia to published values of various materials.

Sorbent	λ_{max} species 1 in nm / fluorescence lifetime in µs	λ_{max} species 2 in nm / fluorescence lifetime in µs	λ_{max} species 3 in nm / fluorescence lifetime in µs	λ_{max} species 4 in nm / fluorescence lifetime in µs
ZrO_2-untreated	600.4 / 85 ± 15	604.1 / 100 ± 20	608.8 / 100 ± 20	613.3 / 140 ± 20
ZrO_2-calc	602.3 / 90 ± 15	606.2 / 90 ± 15	612.5 / 190 ± 40	- / -
Synthetic kaolinite [36]	598.8 / 109 ± 10	602.6 / 116 ± 8	607.4 / -	610.9 / -
Natural kaolinite [67]	598.8 / 116 ± 13	602.2 / 116 ± 13	606.2 / 132 ± 5	609.4 / 132 ± 5
Corundum (α-Al_2O_3) [68]	600.7 / 110 ± 10	603.0 / 110 ± 10	605.4 / 110 ± 10	- / /
γ-Al_2O_3 [69]	600.6 / 110	602.5 / 110	605.7 / 110	- / -
Bayerite [68]	600.6 / 110 ± 10	603.6 / 110 ± 10	606.7 / 110 ± 10	- / -
Gibbsite [70]	603.5 / 135 ± 7	605.6 / 110	- / -	- / -
Silica colloids	602.3 /	604.9 /	- /	- /

[71]	220 ± 14	740 ± 35	-	-

The surface sorbed species distributions for both materials were derived from peak deconvolution. To be able to obtain a relative speciation of the resulting species on both zirconia materials, relative fluorescence intensity factors (f_i^{rel}) for each individual species (i) are required. This is due to the change in the coordination environment of the complexed Cm^{3+} ion in comparison to the aquo ion, causing a shift of the emission maximum ($\lambda_{emission}$) as well as the absorption maximum, which is located at 396.6 nm (used excitation wavelength in the present study) only for the non-complexed aquo ion. To extract such relative fluorescence intensity factors, the overall intensity of the measured emission spectra are compared and normalized to the spectrum of the aquo ion. If some experimental conditions change, such as the overall curium concentration in the sample, the extraction of FI factors is hampered. As a minor amount of the calcined zirconia could be seen to adsorb on the cuvette walls as well as the pH electrode, the extraction of FI factors from the spectroscopic data cannot be achieved under these experimental conditions. Therefore, a new approach for determining the FI factors was brought to use. For this, literature values for FI factors of Cm^{3+} species on various minerals under CO_2-free conditions were plotted together and fitted with an exponential curve (Figure 8). The resulting fit follows equation 2 which was used to calculate the FI factors for the zirconia system.

$$f_i^{rel} = 1.2745 \cdot 10^{38} \cdot \exp\left(-\frac{\lambda_{emission}}{6.773}\right) \qquad (2)$$

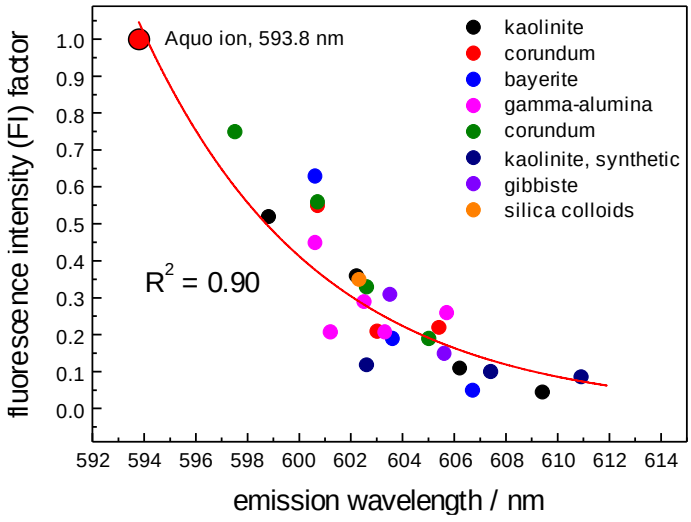

Figure 8: FI factor calibration curve fitted to literature values for kaolinite and synthetic kaolinite [36], corundum [38,68], bayerite [68], γ-alumina [72], gibbsite [70] and silica colloids [71]. An exponential function was used to fit the experimental data.

The resulting FI factors for ZrO_2-untreated are 0.40 for species 1 with its emission maximum of 600.4 nm, 0.23 for species 2 at an emission maximum of 604.1 nm, 0.12 for species 3 and its emission maximum of 608.8 nm and 0.06 for species 4, with an emission maximum of 613.3 nm. For ZrO_2-calc the received value for species 1 with its emission maximum of 602.3 nm is 0.31, for species 2 with an emission maximum of 606.2 nm is 0.17 and for species 3 with an emission maximum of 612.5 nm the fluorescence intensity factor can be determined to be 0.07. It is important to bear in mind that the method described above for determining the FI factors must be seen as approximate with rather high uncertainties. This can be seen when calculating the FI factor for the aquo ion with an emission peak maximum of 593.8 nm resulting in an FI factor of 1.07 using Equation 2. Since the fluorescence intensity factors are normalized to the aquo ion, its FI factor should be equal to 1. The peak positions of species 4 and species 3 of the untreated and the calcined material, respectively, are out of the range for published FI-factors, increasing the uncertainty connected with the values obtained here. In addition, the FI factors of which the calibration curve is based on are for sorption species on inorganic surfaces only, meaning that any species that may be influenced by organics may not be correctly recalculated using our calibration method.

The species distributions of both materials obtained after the FI correction can be seen in Figure 9. In both cases the percentage of the aquo ion is at 100% until a pH of about 3.5 where it starts to decreases until a pH of about 5.5 where no aquo ion can be seen in the spectra anymore. On ZrO_2-untreated, species 1 can be found in a very narrow pH range from about 4 to 5.5 only (Figure 9, left). From a pH of 4.5 onward, species 2 starts to grow in and stays present in a significant amount over a wide pH-range to pH > 9.5. Species 3 can be observed at very similar pH values as species 2 and stays present in the whole pH range from thereon. This species is responsible for the pH-independent behavior seen in Figure 6. Its percentage first peaks at pH ~ 6 with a fraction of 60% and then scatters around a rather constant percentage of about 30%, thus, referred to as the pH-independent species in the following text. At pH-values above 7, a fourth species starts to appear. This species becomes the prevailing one in the alkaline pH-range, above pH ~ 10.

The species distribution on the calcined material ZrO_2-calc shows a comparably systematic decrease and increase of the different species with increasing pH (Figure 9, right). The percentage of the aquo ion is at 100% until a pH of about 3.5 after which it slowly decreases while the first surface sorbed species (species 1) increases, reaching its maximum fraction of 65% at a pH of 5.5. After that species 2 is dominating over a large pH range from pH 7 to pH

10.5 with a maximum fraction of 100% at pH 8.5. Species 3 starts to appear at a pH of 8.9 and increases above the 50% fraction at a pH of 10.5.

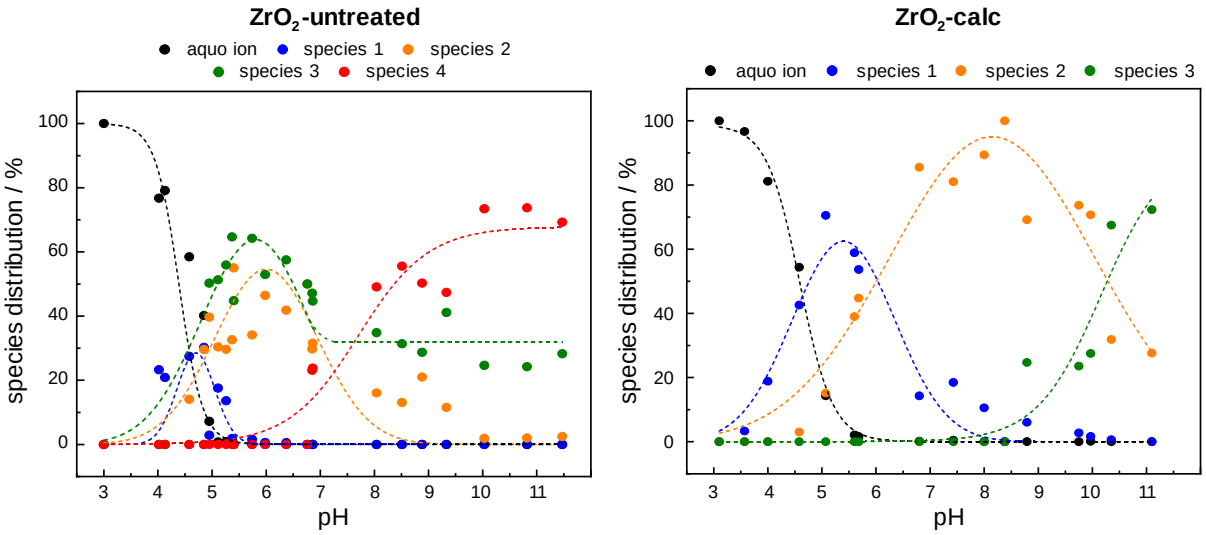

Figure 9: Fluorescence intensity corrected species distributions of Cm^{3+} sorption onto ZrO_2-untreated (left) and ZrO_2-calc (right). The dashed lines are a visualization help only.

The luminescence lifetimes recorded for the Cm^{3+} species in the ZrO_2-untreated suspension show mono-exponential decay for pH-values below 4, followed by multi-exponential decay at higher pH-values (Figure S3, left). In the acidic pH-range a lifetime of 68 ± 2 µs can be obtained by a mono-exponential fit, which corresponds to the lifetime of the Cm^{3+} aquo ion. The multitude of species present in single samples of ZrO_2-untreated in especially in the pH region of 4.5 to 5.5 complicates the determination of luminescence decay constants for each single species. Besides the lifetime of the aquo ion of 68 ± 2 µs, three other lifetimes can be obtained being 85 ± 15 µs, 100 ± 20 µs and 140 ± 20 µs. The short lifetime of 85 ± 15 µs is present in a pH range of 4.5 to 5.5 which correlates with the appearance of species 1 in the species distribution. This corresponds to 7.0 ± 1.4 water molecules in the first hydration sphere, according to *Kimura's* equation. Since every other species appears in mixed systems only, any further assignment is rather speculative. However, it seems that species 2 and species 3 have rather similar lifetimes of around 100 µs, correlating to 5.8 ± 1.4 water molecules while species 4 seems to show the longest lifetimes of 140 ± 20 µs ($N(H_2O)$ = 4.0 ± 0.8).

Due to the low suspension stability of the ZrO_2-calc material, the recorded lifetimes for this system are rather scattered (Figure S3, right). Nevertheless, the lifetimes derived from bi-exponential fits of the Cm^{3+} luminescence decay of sorption species on ZrO_2-calc give two lifetimes distinct from the one of the aquo ion, being 90 ± 20 µs which can be assigned to species 1 and 2 which have rather similar luminescence decay behavior and 190 ± 40 µs

which correlates with species 3 present at high pH values. The lifetimes of species 1 and 2 are in a similar range as the lifetimes obtained from ZrO_2-untreated, while the lifetime of species 3 seems to correlate with that of species 4 in the pristine system. Given the large errors of the luminescence lifetimes, the number of hydration water molecules can be estimated only roughly to be 7 ± 1.7 for species 1, 6 ± 1.7 for species 2, and 3 ± 1 for species 3.

3.3. Speciation Modelling

The Diffuse Double Layer model has been used to describe the sorption process. The obtained set of surface complexation modelling parameters is given in Table 3.

Table 3: Parameter set for surface complexation modelling of Cm^{3+} sorption onto calcined ZrO_2.

Model parameter	Value	Ref.
Site density [nm^{-2}]	7.56	This work
Protolysis constant 1 ($pK_{a1}°$)	4.0	[60]
Protolysis constant 2 ($pK_{a2}°$)	8.1	[60]
Formation constant for Cm^{3+} species 1 ($\log_{10}K°$)	-3.04	This work
Formation constant for Cm^{3+} species 2 ($\log_{10}K°$)	-9.04	This work
Formation constant for Cm^{3+} species 3 ($\log_{10}K°$)	-22.45	This work

The calculated SSD value is in good agreement with values from Jung and Bell [73] who report a value of 6.2 OH surface groups per nm^2 surface area for a similar, monoclinic zirconia sample.

The FI-corrected species distribution obtained for Cm^{3+} sorption on the calcined zirconia (ZrO_2-calc) was used to obtain the surface complexation constants. Figure 10, left shows the modelled species distribution (lines) together with the experimental data points (filled symbols). The obtained surface complexation constants were thereafter used to model the resulting Cm^{3+} pH-edge, obtained by subtracting the percentage of adsorbed species from the aquo ion (line in Figure 10, right). Even though a rather good match between the modelled pH-edge (solid line) and the experimental data (filled symbols) is achieved, the species distribution clearly shows a discrepancy for species 2 and species 3. Assuming bidentate

coordination to the zirconia surface (coordination to surface assumed to be the difference between the overall coordination number of 9 and the number of coordinating water molecules which were estimated to be 7 from the obtained luminescence lifetime data), species 2 is clearly underestimated by this model. The opposite is true for species 3, which is overestimated by the surface complex coordinated to five surface hydroxyls on the zirconia surface. It can be excluded, that differences of the surface deprotonation cause the discrepancies between the modelled and the experimental data, as the degree of deprotonation of the participating surface hydroxyl groups has been varied in the model to include every chemically reasonable case.

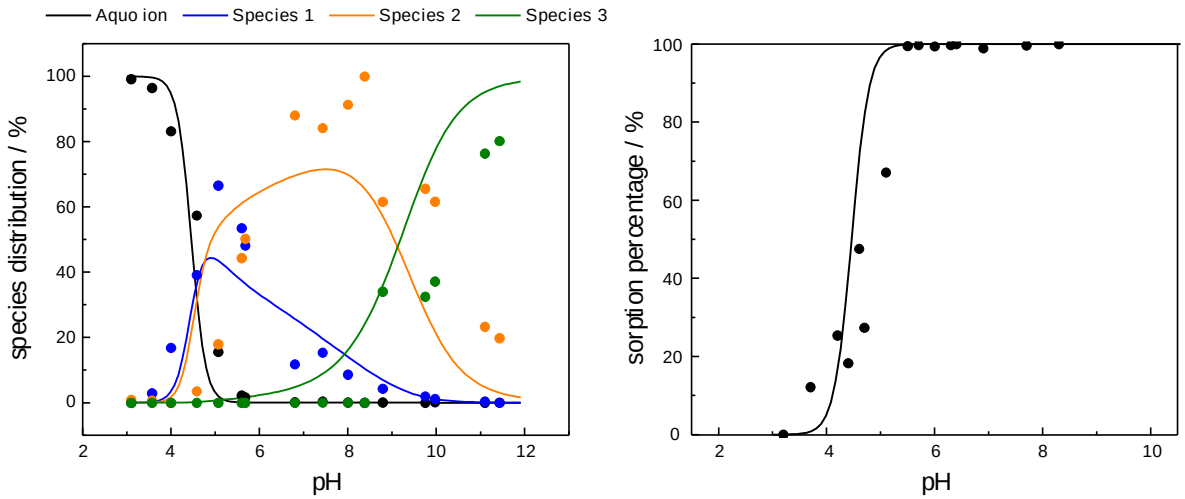

Figure 10: Comparison of the modelled species distribution (lines) to the experimental data (filled symbols) (left) and resulting sorption edge for Cm^{3+} sorption onto calcined ZrO_2 (line) in comparison to the experimental data (filled symbols) (right).

4. Discussion

Both zirconium oxide materials used in the present study, although originating from the same starting material, reveal significant differences in their surface and sorption properties.

Even though the SEM-EDX and BET investigations showed that the particle size and the micro pore volume of both the untreated mineral and the calcined product are very similar, the BET surface area of ZrO_2-untreated was found to be almost four times larger than the one of ZrO_2-calc. The lower surface area of the calcined product may be a result of the high agglomeration tendency of the material in comparison to the pristine one, however, the presence of rather significant amounts of both organic and inorganic carbon in the untreated product may contribute to the overall larger surface area of this material.

The carbon content could be considerably reduced through calcination even though small amounts of carbon were measured in the TC survey of the calcined zirconia. Due to storage of both minerals under ambient conditions, it can be assumed that this carbon source is re-adsorbed CO_2 from air forming inorganic carbonate species on the zirconia surface. Such carbonate adsorption could be shown to influence the surface charge of the solid phases. In the presence of atmospheric carbon dioxide, the IEP of the untreated solid decreased from pH_{IEP} = 9 (at inert conditions) to approximately 7, while a slight increase from pH_{IEP} = 6 (at inert conditions), again to approximately 7 was found for the calcined product.

The comparison of both materials at inert conditions (Figure S1, top) shows a large difference of the IEP, although, when the measured suspensions are prepared at ambient conditions they both show a pH_{IEP} of 7.

Since both materials have been stored at ambient conditions and have therefore been in contact with ambient CO_2 but still show a strong difference in their IEP it can be deduced that the organics are the major source of influence here. Arguably, a differing storage time in ambient conditions after calcination could alter the carbonate species concentration on the surface. However, the chemisorption of acidic CO_2 is expected to lower the pH_{IEP} but still, ZrO_2-untreated has a much higher IEP at inert conditions than ZrO_2-calc. Therefore, it can be deduced that the organic contaminant has a strong influence on the surface charge of the material.

That both samples show a very similar pH_{IEP} when prepared at ambient conditions shows that the comparably high carbonate concentration, caused by the dissolution of atmospheric CO_2 especially in high pH suspensions, outweighs the surface charge effects, caused by sorbed organic carbon, visible at inert conditions.

The different pH-dependent surface charges of the minerals under inert conditions could not be seen to significantly impact the pH-dependent adsorption of Eu^{3+} in the batch sorption experiments. On the other hand, large differences in the metal ion speciation could be observed in the spectroscopic studies. Here, the deconvolution of recorded Cm^{3+} emission spectra in the ZrO_2-untreated suspension resulted in four sorption species while only three could be found on ZrO_2-calc. Based on the obtained species distribution from the deconvoluted spectroscopic data, a very untypical, non-pH dependent species was identified on the ZrO_2-untreated surface. The amount of this species (species 3) scatters around a constant value of about 30% over the range from pH 7 to 11.5 (Figure 9, left). The relative amounts of the three additional surface complexes (species 1, species 2, and species 4),

however, do strongly depend on the pH of the suspension. Such pH-dependent formation of multiple Cm-surface complexes on minerals has been shown to arise from hydrolysis reactions and the adsorption of such hydrolyzed species on the mineral surface in the absence of carbonate (see e.g. [36,37,68,69]).

To be able to compare the pH-dependent speciation of Cm^{3+} sorption on ZrO_2-untreated and ZrO_2-calc, and potentially relate this pH-dependent evolution of the participating species to Cm^{3+}-hydrolysis, the pH-independent species (species 3) was neglected from the species distribution in the ZrO_2-untreated suspension and the resulting speciation plot was compared to the Cm^{3+} speciation on ZrO_2-calc (Figure 11).

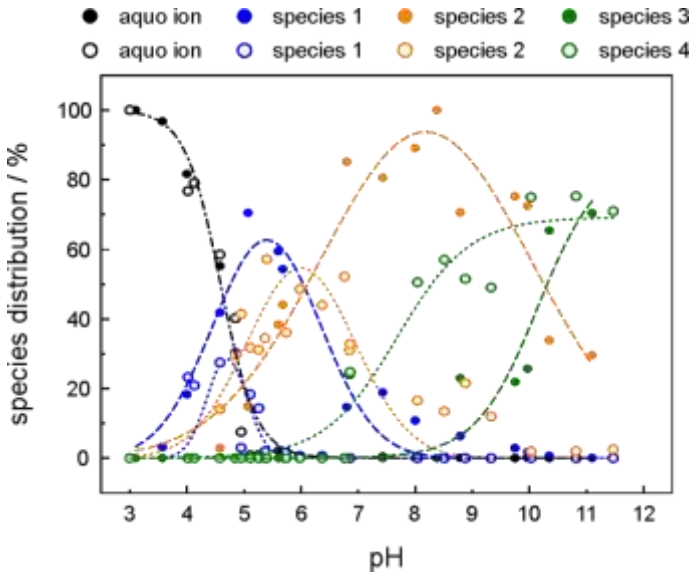

Figure 11: Species distribution of the Cm^{3+} sorption on ZrO_2-calc (filled symbols and dashed lines) and on ZrO_2-untreated, neglecting the pH-independent species (open symbols and dotted lines). Note that the overall percentage from a pH of about 4 does not sum up to 100% since species 3 is excluded. The dashed and dotted lines are a visualization help only.

The overall percentages of the pH-dependent species on the ZrO_2-untreated surface are lower than on ZrO_2-calc due to the presence of the additional pH-independent species in this system (see Figure 9, left). However, when comparing the pH-range where the formation of each pH-dependent species occurs, similarities can be found in both systems. The measured lifetimes for these species are also similar with lifetimes of 85 and 100 µs for species 1 and species 2 on ZrO_2-untreated compared to an average of 90 µs for these complexes on ZrO_2-calc. For species 3 (ZrO_2-calc) and species 4 (ZrO_2-untreated), lifetimes of 190 and 140 µs, respectively were obtained. Therefore, there are reasons to believe that these species are similar Cm^{3+}-surface complexes on both zirconia materials, where species 1 is a non-hydrolyzed Cm^{3+} complex, species 2 the first hydrolysis species sorbed on the respective

minerals and species 3 (ZrO_2-calc) / species 4 (ZrO_2-untreated) the second surface sorbed hydrolysis complex. This assignment is done despite the fact that the Cm^{3+} emission peak positions of the pure component spectra obtained for the two minerals are different (see Figure 7). These differences of the peak positions can arise from the species deconvolution for example. Because of the large number of species present in a narrow pH-range in especially on ZrO_2-untreated the derived single species spectra contain a degree of uncertainty because the derived species are co-dependent of each other. Furthermore, the presence of organic contaminants on ZrO_2-untreated could have a slight influence on the Cm^{3+} environment of adsorbed species, leading to small changes in their emission peak positions in comparison to a contaminant-free surface (ZrO_2-calc).

When looking at the absolute values of the emission peak positions, especially for the calcined product where uncertainties related to the peak positions are smaller than for the untreated product, rather untypically red-shifted spectra are obtained in comparison to the free aquo ion at 593.8 nm. Species 3 of the calcined material as well as species 4 on ZrO_2-untreated show extraordinarily strong red shifts with peak positions of 612.5 nm and 613.3 nm, respectively. The most red shifted sorption species found for different materials are reported at wavelengths of 605.7 nm on γ-Al_2O_3,[69] 607.1 nm on Ca-montmorillonite [12] or 607.5 nm on calcite [74] to give just a few examples.

A strong red-shift, i.e. a smaller energy difference between the emitting level and the ground state, means that Cm^{3+} is influenced by a strong ligand field. A strong ligand field may arise from e.g. a high coordination to the surface or an untypically short Cm-O bonding to the surface.

Nonetheless, other reasons such as partial incorporation of Cm^{3+} into the mineral must be considered as well. The solubility of ZrO_2 is very poor even at pH values between 9 and 12, where species 3 is observed.[75] However, it could be seen that the surface of zirconia shows a very high reactivity due to a high concentration of unsaturated valences on the surface which leads to a strong adsorption of ions and molecules in its environment, such as Cm^{3+} or water.[76] The dissociative adsorption of water leads to an alteration of the surface, resulting in surface layers of very differing properties to the bulk material. This surface alteration effect could be enhanced by organic species present on the surface or in the bulk yielding a less crystalline product and therefore making it easier to break down deeper layers of the bulk. Consequently species 4 found on ZrO_2-untreated and species 3 on ZrO_2-calc could be the

result of a partial incorporated species into such amorphous surface layers on the zirconia solids.

So far the discussion of the pH-independent species (species 3) on the ZrO_2- untreated surface was omitted. This species occurs already in the acidic pH range (pH ~ 5), and has an unusually red-shifted peak position of 608.4 nm. Such peak positions have never been recorded for inorganic Cm^{3+}-complexes on mineral surfaces in the acidic pH-range, which is why it is assumed here, that this species is a Cm^{3+} complex formed between Cm^{3+} and the organic contaminant present on the ZrO_2-untreated surface. Furthermore, Cm-complexation with organics has been shown to cause rather pronounced red-shifts of the recorded emission spectra.[77–79] However, due to the nearly complete removal of trivalent metals from solution at pH values above 5 (see Figure 4) this organic-bound Cm^{3+} complex cannot be a solution species but must be adsorbed on the zirconia surface.

The surface complexation modeling in the present study was based on the surface speciation obtained for Cm^{3+} sorption on the calcined zirconia surface. The surface denticity of the modeled species were taken from the collected lifetime data in our laser spectroscopic investigations. As previously mentioned, lifetimes of species 1 and 2 on the zirconia solids ranged from 85 to 100 µs corresponding to 7 and 6 water molecules (rounded values are used) in the first hydration sphere of the actinide cation. To preserve an overall coordination number of 9, bidentate and tridentate coordination to the surface must occur for species 1 and species 2, respectively. The long lifetime for species 4 (ZrO_2-untreated) and 3 (ZrO_2-calc) with an average value of 165 ± 25 µs corresponds to 3.2 ± 0.6 water molecules. Therefore, a higher surface coordination is to be expected. Assuming that –OH entities of a hydrolyzed Cm^{3+} cation have a slightly lower luminescence quenching effect than H_2O molecules (non-hydrolyzed Cm^{3+}) we assumed a penta-dentate surface coordination for this species in the modeling. As discussed in the previous paragraph, such high coordination of Cm^{3+} to the surface might indeed explain the strongly red-shifted emission spectra recorded in our laser spectroscopic investigations. As seen in Figure 10, the surface complexation model reproduces the experimentally determined Cm^{3+} sorption edge rather well. From the experimentally derived species distribution (Figure 9), it is evident that the edge position is influenced mainly by species 1.

The modeled species distribution, however, differs significantly from the experimentally determined one with regard to species 2 and 3. Since the assumed surface species, for which the formation constants were fitted, are based only on the information on the amount of water

molecules in the first hydration sphere and the probable number of surface groups bound in the complex, the speciation is associated with a high degree of uncertainty.

Especially species 3 is highly overestimated by our model. This may be due to an over/underestimation of the surface coordination, however, discrepancies in the actual uptake mechanism and participating ligands may play an important role as well. The modeled Cm^{3+} species is assumed to be an ordinary surface complex coordinating to surface hydroxyls only. We know from the total carbon measurements that a carbon impurity, most likely, re-adsorbed CO_2 is present on the ZrO_2-calc surface. Carbonate species are known to form ternary surface complexes with trivalent Eu^{3+} and Cm^{3+} ions [80,81] resulting in rather long luminescence lifetimes due to the replacement of H_2O/OH^- entities by the carbonate ligand in the metal ion coordination spheres. Such an increase of the recorded lifetime due to the presence of carbonates on the mineral surface, would lead to an overestimation of the surface coordination predicted based on the number of H_2O/OH^- entities in the Cm^{3+} coordination sphere and further to an erroneous description of the surface complexation reaction used in our model. Another potential reaction leading to an incorrect surface complexation model is the previously discussed partial incorporation of Cm^{3+} in an amorphous layer forming on the zirconia surface. Thus, in order to improve the model, additional information of the Cm^{3+} speciation on ZrO_2 would be required. For this, future studies providing information of the metal ion coordination sphere, such as x-ray absorption spectroscopy are planned to access the lacking data required for such a refinement of our surface complexation model.

5. Conclusions and Outlook

As the major corrosion product of the zircaloy cladding material, the retention potential of ZrO_2 towards released radioactive contaminants from spent nuclear fuel needs to be understood in detail. Thus, the present study focused on understanding the uptake of trivalent metal cations, including the actinide Cm^{3+}, by monoclinic zirconia, which is expected to be the most stable polymorph of ZrO_2 under repository conditions. Moreover, as the ZrO_2 surface is known to adsorb both inorganic and organic carbon species, which may alter the retention of metal ions on the mineral and their speciation on the surface, two different zirconia solids varying in their carbon content were used in parallel. The presence of both organic and inorganic carbon impurities were detected on the non-treated zirconia surface. Upon calcination, a large fraction of the total carbon concentration was removed, implying that sample pretreatment may be crucial to avoid artefacts caused by the presence of undesired impurities. The impurity on the ZrO_2-untreated material was found to influence the electrophoretic mobility in terms of the measured zeta-potential in comparison to the heat-treated material with less carbon contamination, resulting in an isoelectric point (IEP) at pH = 9.0 for ZrO_2-untreated in contrast to pH = 5.8 for ZrO_2-calc. Despite of the rather different surface charges, the pH-dependent sorption of Eu^{3+} investigated in our batch-sorption studies showed no noteworthy differences for the two zirconia materials. Eu^{3+} was retained by both minerals in the mildly acidic pH-range (from pH 4 – 5.5) and above, indicating an excellent retention potential of the material toward trivalent contaminants. A similar conclusion was reached by Salem and Yakout [82] investigating Er^{3+} removal by sol–gel-derived zirconia, where the endothermic sorption reaction reached maximum Er^{3+} uptake at pH > 5 under the given experimental conditions.

Our spectroscopic investigations using the luminescent actinide Cm^{3+} showed that the carbon source on the untreated ZrO_2 surface has a large influence on the Cm^{3+} speciation, with results suggesting the formation of a Cm-organo-complex on the solid surface. On the ZrO_2 material free of organic contaminants, three pH-dependent Cm^{3+} surface species were observed and their single species spectra, lifetimes, and species distribution were derived. Based on the experimental species distribution and the presumed surface speciation, surface complexation modeling using the Diffuse Double Layer model was conducted. Here, a good description of the surface complexes occurring in the neutral to alkaline pH-range could not be achieved, implying that additional processes such as carbonate complexation or partial incorporation of Cm^{3+} in the amorphous surface layers of zirconia may play a role in the metal ion speciation. Our spectroscopic results are the first to describe trivalent metal ion speciation on the ZrO_2

surface. In addition, the surface complexation model has provided the first surface complexation constants quantifying the pH-dependent adsorption reaction of trivalent actinides on zirconia. Furthermore, the macroscopic uptake behavior observed in the experiments was in good agreement with the modelled sorption edge. In the future, the role of remaining trace carbonate species on the zirconia surface and their role in the actinide speciation must be clarified. In this context, re-adsorption of CO_2 from air on the mineral surface should be prevented by calcination of zirconia under an inert gas atmosphere followed by storage of the material in N_2/Ar glove boxes to help preserve a pristine mineral surface free of re-adsorbed carbon species. This may help elucidating the involvement of actinide incorporation reactions at the zirconia interface, especially when combining the sorption investigations on a fully carbon-free surface with spectroscopic methods sensitive to the surrounding actinide environment, such as x-ray absorption methods.

Finally, in a waste repository for SNF, both inorganic and organic carbon sources will be present. The concentration of soluble carbon species will vary and depend on the various microbial and geochemical processes taking place in the deep underground. Organic material will be introduced in plastics, cellulose, surfactants, and cement additives and can be found as e.g. humic and fulvic acids in buffer and backfill materials. The main inorganic carbon sources are natural carbonate-containing minerals, cementitious barriers and grout. Thus, future studies should include ternary systems, where organic substances or carbonates are deliberately added to the investigated system, for a better understanding of the behavior of actinides at the zirconia interface.

Acknowledgements

The authors would like to thank Dr. Atsushi Ikeda for assistance with PXRD measurements. Sabrina Gurlit and Carola Eckardt are thanked for ICP-MS analyses and TC, TOC and TIC determinations, respectively. We also want to thank John Waters and Heath Bagshaw for the BET analysis as well as assistance with EDX-SEM measurements.

This work was supported by the Finnish Doctoral Programme for Nuclear Engineering and Radiochemistry (YTERA) and by the graduate academy of the *Technische Universität Dresden* from funds of the "*Exzellenzinitiative*" of the German state and federal states.

References

[1] A.T. Motta, A. Couet, R.J. Comstock, Corrosion of Zirconium Alloys Used for Nuclear Fuel Cladding, Annu. Rev. Mater. Res. 45 (2015) 311–343. doi:10.1146/annurev-matsci-070214-020951.

[2] B. Cox, Some thoughts on the mechanisms of in-reactor corrosion of zirconium alloys, J. Nucl. Mater. 336 (2005) 331–368. doi:10.1016/j.jnucmat.2004.09.029.

[3] F. Claret, T. Schäfer, T. Rabung, M. Wolf, A. Bauer, G. Buckau, Differences in properties and Cm(III) complexation behavior of isolated humic and fulvic acid derived from Opalinus clay and Callovo-Oxfordian argillite, Appl. Geochem. 20 (2005) 1158–1168. doi:10.1016/j.apgeochem.2005.01.008.

[4] J.D. Prikryl, A. Jain, D.R. Turner, T. Pabalan, Uranium(VI) sorption behavior on silicate mineral mixtures, J. Contam. Hydrol. 47 (2001) 241–253. doi:10.1016/S0169-7722(00)00153-4.

[5] E. Hartmann, B. Baeyens, M.H. Bradbury, H. Geckeis, T. Stumpf, A Spectroscopic Characterization and Quantification of M(III)/Clay Mineral Outer-Sphere Complexes., Environ. Sci. Technol. 42 (2008) 7601–7606. doi:10.1021/es801092f.

[6] E. Hartmann, H. Geckeis, T. Rabung, J. Lützenkirchen, T. Fanghänel, Sorption of radionuclides onto natural clay rocks, Radiochim. Acta. 96 (2008) 699–707. doi:10.1524/ract.2008.1556.

[7] D.I. Kaplan, T.L. Gervais, K.M. Krupka, Uranium(VI) Sorption to Sediments Under High pH and Ionic Strength Conditions, Radiochim. Acta. 80 (1998) 201–211. doi:10.1524/ract.1998.80.4.201.

[8] A. Schnurr, R. Marsac, T. Rabung, J. Lützenkirchen, H. Geckeis, Sorption of Cm(III) and Eu(III) onto clay minerals under saline conditions: Batch adsorption, Laser-fluorescence spectroscopy and modeling, Geochim. Cosmochim. Acta. 151 (2015) 192–202. doi:10.1016/j.gca.2014.11.011.

[9] C. Joseph, K. Schmeide, S. Sachs, V. Brendler, G. Geipel, G. Bernhard, Sorption of uranium(VI) onto Opalinus Clay in the absence and presence of humic acid in Opalinus Clay pore water, Chem. Geol. 284 (2011) 240–250. doi:10.1016/j.chemgeo.2011.03.001.

[10] C. Joseph, M. Stockmann, K. Schmeide, S. Sachs, V. Brendler, G. Bernhard, Sorption of U(VI) onto Opalinus Clay: Effects of pH and humic acid, Appl. Geochem. 36 (2013) 104–117. doi:10.1016/j.apgeochem.2013.06.016.

[11] M.H. Bradbury, B. Baeyens, Experimental measurements and modeling of sorption competition on montmorillonite, Geochim. Cosmochim. Acta. 69 (2005) 4187–4197. doi:10.1016/j.gca.2005.04.014.

[12] T. Rabung, M.C. Pierret, A. Bauer, H. Geckeis, M.H. Bradbury, B. Baeyens, Sorption of Eu(III)/Cm(III) on Ca-montmorillonite and Na-illite. Part 1: Batch sorption and time-resolved laser fluorescence spectroscopy experiments, Geochim. Cosmochim. Acta. 69 (2005) 5393–5402. doi:10.1016/j.gca.2005.06.030.

[13] D.R. Turner, T.R. Pabalan, F.P. Bertetti, Neptunium(V) Sorption on Montmorillonite: An Experimental and Surface Complexation Modeling Study, Clays Clay Miner. 46 (1998) 256–269. doi:10.1346/CCMN.1998.0460305.

[14] M.N. Sabodina, S.N. Kalmykov, Y.A. Sapozhnikov, E.V. Zakharova, Neptunium, plutonium and Cs-137 sorption by bentonite clays and their speciation in pore waters, J. Radioanal. Nucl. Ch. 270 (2006) 349–355. doi:10.1007/s10967-006-0356-6.

[15] H. Akçay, Aqueous speciation and pH effect on the sorption behavior of uranium by montmorillonite, J. Radioanal. Nucl. Ch. 237 (1998) 133–137. doi:10.1007/BF02386676.

[16] C.J. Chisholm-Brause, J.M. Berg, K.M. Little, R.A. Matzner, D.E. Morris, Uranyl sorption by smectites: spectroscopic assessment of thermodynamic modeling, J. Colloid Interf. Sci. 277 (2004) 366–382. doi:10.1016/j.jcis.2004.04.047.

[17] M.H. Bradbury, B. Baeyens, Modelling the sorption of Mn(II), Co(II), Ni(II), Zn(II), Cd(II), Eu(III), Am(III), Sn(IV), Th(IV), Np(V) and U(VI) on montmorillonite: Linear free energy relationships and estimates of surface binding constants for some selected heavy metals and actinides, Geochim. Cosmochim. Acta. 69 (2005) 875–892. doi:10.1016/j.gca.2004.07.020.

[18] J.G. Catalano, E. Brown Jr., Uranyl adsorption onto montmorillonite: Evaluation of binding sites and carbonate complexation, Geochim. Cosmochim. Acta. 69 (2005) 2995–3005. doi:10.1016/j.gca.2005.01.025.

[19] S. Bachmaf, B. Planer-Friedrich, B.J. Merkel, Effect of sulfate, carbonate, and phosphate on the uranium(VI) sorption behavior onto bentonite, Radiochim. Acta. 96 (2008) 359–366. doi:10.1524/ract.2008.1496.

[20] A. Meleshyn, M. Azeroual, T. Reeck, G. Houben, B. Riebe, C. Bunnenberg, Influence of (Calcium−)Uranyl−Carbonate Complexation on U(VI) Sorption on Ca- and Na-Bentonites, Environ. Sci. Technol. 43 (2009) 4896–4901. doi:10.1021/es900123s.

[21] P. Ivanov, T. Griffiths, T. Bryan, G. Bozhikov, S. Dmitriev, The effect of humic acid on uranyl sorption onto bentonite at trace uranium levels, J. Environ. Monitor. 14 (2012) 2968–2975. doi:10.1039/C2EM30512G.

[22] M. Marques Fernandes, B. Baeyens, R. Dähn, A.C. Scheinost, M.H. Bradbury, U(VI) sorption on montmorillonite in the absence and presence of carbonate: A macroscopic and microscopic study, Geochim. Cosmochim. Acta. 93 (2012) 262–277. doi:10.1016/j.gca.2012.04.017.

[23] P.K. Verma, P. Pathak, M. Mohapatra, A.K. Yadav, S. Jha, D. Bhattacharyya, P.K. Mohapatra, Spectroscopic investigations on sorption of uranium onto suspended bentonite: effects of pH, ionic strength and complexing anions, Radiochim. Acta. 103 (2015) 293–303. doi:10.1515/ract-2014-2309.

[24] X. Tan, M. Fang, X. Wang, Sorption Speciation of Lanthanides/Actinides on Minerals by TRLFS, EXAFS and DFT Studies: A Review, Molecules. 15 (2010) 8431–68. doi:10.3390/molecules15118431.

[25] M.H. Bradbury, B. Baeyens, Sorption modelling on Illite. Part II: Actinide sorption and linear free energy relationships, Geochim. Cosmochim. Acta. 73 (2009) 1004–1013. doi:10.1016/j.gca.2008.11.016.

[26] M.H. Bradbury, B. Baeyens, Predictive sorption modelling of Ni(II), Co(II), Eu(III), Th(IV) and U(VI) on MX-80 bentonite and Opalinus Clay: A “bottom-up” approach, Appl. Clay Sci. 52 (2011) 27–33. doi:10.1016/j.clay.2011.01.022.

[27] B. Kienzler, P. Vejmelka, J. Römer, E. Fanghänel, M. Jansson, T. Eriksen, P. Wikberg, Swedish-German actinide migration experiment at ASPO hard rock laboratory, J. Contam. Hydrol. 61 (2003) 219–233. doi:10.1016/S0169-7722(02)00133-X.

[28] B. Allard, G.W. Beall, T. Krajewski, The Sorption of Actinides in Igneous Rocks, Nucl. Technol. 49 (1982) 474–480. doi:10.13182/NT80-A17695.

[29] M.H. Baik, S.P. Hyun, W.J. Cho, P.S. Hahn, Contribution of minerals to the sorption of U(VI) on granite, Radiochim. Acta. 92 (2004) 663–669. doi:10.1524/ract.92.9.663.54980.

[30] M.S. Murali, J.N. Mathur, Sorption characteristics of Am(III), Sr(II) and Cs(I) on bentonite and granite, J. Radioanal. Nucl. Ch. 254 (2002) 129–136. doi:10.1023/A:1020858001845.

[31] J.L. Means, D.A. Crear, P. Borcsik, J.O. Duguid, Adsorption of Co and selected actinides by Mn and Fe oxides in soils and sediments, Geochim. Cosmochim. Acta. 42 (1978) 1763–1773. doi:10.1016/0016-7037(78)90233-8.

[32] R.J. Murphy, J.J. Lenhart, B.D. Honeyman, The sorption of thorium (IV) and uranium (VI) to hematite in the presence of natural organic matter, Colloid. Surface. A. 157 (1999) 47–62. doi:10.1016/S0927-7757(99)00115-6.

[33] A.B. Kashanova, S.N. Kalmykov, I.V. Perminova, S.B. Clark, Neptunium redox behavior and sorption onto goethite and hematite in the presence of humic acids with different hydroquinone content, J. Alloy. Compd. 444–445 (2007) 491–494. doi:10.1016/j.jallcom.2007.02.069.

[34] A.Y. Romanchuk, S.N. Kalmykov, R.A. Aliev, Plutonium sorption onto hematite colloids at femto- and nanomolar concentrations, Radiochim. Acta. 99 (2011) 1–8. doi:10.1524/ract.2011.1808.

[35] W. Runde, The Chemical Interactions of Actinides in the Environment, Los Alamos Sci. 26 (2000) 392–411.

[36] N. Huittinen, T. Rabung, P. Andrieux, J. Lehto, H. Geckeis, A comparative batch sorption and time-resolved laser fluorescence spectroscopy study on the sorption of Eu(III) and Cm(III) on synthetic and natural kaolinite, Radiochim. Acta. 98 (2010) 613–620. doi:10.1524/ract.2010.1761.

[37] N. Huittinen, T. Rabung, J. Lützenkirchen, S.C. Mitchell, B.R. Bickmore, J. Lehto, H. Geckeis, Sorption of Cm(III) and Gd(III) onto gibbsite, α-$Al(OH)_3$: A batch and TRLFS study, J. Colloid Interf. Sci. 332 (2009) 158–64. doi:10.1016/j.jcis.2008.12.017.

[38] S. Virtanen, S. Meriläinen, M. Eibl, T. Rabung, J. Lehto, N. Huittinen, Sorption competition and kinetics of trivalent cations (Eu, Y and Cm) on corundum (α-Al_2O_3): A batch sorption and TRLFS study, Appl. Geochem. 92 (2018) 71–81. doi:10.1016/j.apgeochem.2018.02.011.

[39] N. Janot, M.F. Benedetti, P.E. Reiller, Colloidal α-Al_2O_3 Europium(III) and humic substances interactions: a macroscopic and spectroscopic study, Environ. Sci. Technol. 45 (2011) 3224–30. doi:10.1021/es102592a.

[40] T. Rabung, D. Schild, H. Geckeis, R. Klenze, T. Fanghänel, Cm(III) Sorption onto Sapphire (α-Al_2O_3) Single Crystals, J. Phys. Chem. B. 108 (2004) 17160–17165. doi:10.1021/jp040342h.

[41] M.C. Duff, J.U. Coughlin, D.B. Hunter, Uranium co-precipitation with iron oxide minerals, Geochim. Cosmochim. Acta. 66 (2002) 3533–3547. doi:10.1016/S0016-7037(02)00953-5.

[42] I. Rojo, F. Seco, M. Rovira, J. Giménez, G. Cervantes, V. Martí, J. de Pablo, Thorium sorption onto magnetite and ferrihydrite in acidic conditions, J. Nucl. Mater. 385 (2009) 474–478. doi:10.1016/j.jnucmat.2008.12.014.

[43] K. Nakata, S. Nagasaki, S. Tanaka, Y. Sakamoto, T. Tanaka, H. Ogawa, Reduction rate of neptunium(V) in heterogeneous solution with magnetite, Radiochim. Acta. 92 (2004). doi:10.1524/ract.92.3.145.30493.

[44] H.E. Roberts, K. Morris, G.T.W. Law, J.F.W. Mosselmans, P. Bots, K. Kvashnina, S. Shaw, Uranium(V) Incorporation Mechanisms and Stability in Fe(II)/Fe(III) (oxyhydr)Oxides, Environ. Sci. Technol. Let. 4 (2017) 421–426. doi:10.1021/acs.estlett.7b00348.

[45] C. Lomenech, R. Drot, E. Simoni, Speciation of uranium(VI) at the solid/ solution interface: sorption modeling on zirconium silicate and zirconium oxide, Radiochim. Acta. 91 (2003) 453–461.

[46] H.S. Mahal, B. Venkataramani, K.S. Venkateswarlu, Sorption Properties of Oxides VIII: Sorption of Uranium on Hydrous Oxides, J. Inorg. Nucl. Chem. 43 (1981) 3335–3342.

[47] L. Maya, Sorbed Uranium(VI) Species on Hydrous Titania, Zirconia, and Silica Gel, Radiochim. Acta. 31 (1982) 147–151.

[48] R.D. Bhanushali, S.S. Pathak, I.C. Pius, S.K. Mukerjee, Recovery of plutonium from aqueous waste solutions using porous zirconia spherical particles, J. Radioanal. Nucl. Ch. 285 (2010) 647–651. doi:10.1007/s10967-010-0590-9.

[49] I.A. Korshunov, N.G. Chernorukov, T.V. Prokof'eva, Neptunium and plutonium sorption on some hardly soluble compounds, Radiokhimiya. 18 (1976).

[50] A. Hedin, Spent nuclear fuel - how dangerous is it? A report from the project "Description of risk," Swedish Nuclear Fuel and Waste Management Co, Stockholm, Sweden, 1997.

[51] S. Block, J.A.H. Jornada, G.J. Piermarini, Pressure-Temperature Phase Diagram of Zirconia, J. Am. Ceram. Soc. 68 (1985) 497–499. doi:10.1111/j.1151-2916.1985.tb15817.x.

[52] M. Kosmulski, The pH-dependent surface charging and the points of zero charge, J. Colloid Interf. Sci. 253 (2002) 77–87. doi:10.1006/jcis.2002.8490.

[53] K. Tanabe, Surface and Catalytic Properties of ZrO_2, Mater. Chem. Phys. 13 (1985) 347–364. doi:10.1016/0254-0584(85)90064-1.

[54] B. Bachiller-Baeza, I. Rodriguez-Ramos, A. Guerrero-Ruiz, Interaction of Carbon Dioxide with the Surface of Zirconia Polymorphs, Langmuir. 14 (1998) 3556–3564. doi:10.1021/la970856q.

[55] L.D. David, Production of Metastable Tetragonal Zirconia, Pt. Nr. 4520114, 1985.

[56] P. Scherrer, Bestimmung der Größe und der inneren Struktur von Kolloidteilchen mittels Röntgenstrahlen, Göttinger Nachrichten Math. Phys. 2 (1918) 98–100.

[57] T. Kimura, G.R. Choppin, Y. Kato, Z. Yoshida, Determination of the Hydration Number of Cm(III) in Various Aqueous Solutions, Radiochim. Acta. 72 (1996) 61–64. doi:10.1524/ract.1996.72.2.61.

[58] C.F. Macrae, I.J. Bruno, J.A. Chisholm, P.R. Edgington, P. McCabe, E. Pidcock, L. Rodriguez-Monge, R. Taylor, J. van de Streek, P.A. Wood, Mercury CSD 2.0 - New Features for the Visualization and Investigation of Crystal Structures, J. Appl. Crystallogr. 41 (2008) 466–470. doi:10.1107/S0021889807067908.

[59] D.K. Smith, W. Newkirk, The crystal structure of baddeleyite (monoclinic ZrO_2) and its relation to the polymorphism of ZrO_2, Acta Crystallogr. 18 (1965) 983–991. doi:10.1107/S0365110X65002402.

[60] J.A. Blackwell, P.W. Carr, A Chromatographic Study of the Lewis Acid-Base Chemistry of Zirconia Surfaces, J. Liq. Chromatogr. 14 (1991) 2875–2889. doi:10.1080/01483919108049363.

[61] E.P. Poeter, M.C. Hill, E.B. Banta, S. Mehl, S. Christensen, UCODE_2005 and Six Other Computer Codes for Universal Senitivity Analysis, Calibration, and Uncertainty Evaluation: U.S. Geological Survey Techniques and Methods 6-A11, Reston, Virginia, 2005.

[62] D.L. Parkhurst, C.A.J. Appelo, Description of input and examples for PHREEQC version 3 - A computer program for speciation, batch-reaction, one-dimensional transport, and inverse geochemical calculations: U.S. Geological Survey Techniques and Methods, Book 6, Chap. A43, in: Modeling Techniques, 2013.

[63] T. Thoenen, W. Hummel, U. Berner, E. Curti, The PSI/Nagra Chemical Thermodynamic Database 12/07 - Nuclear Energy and Safety Research Department Laboratory for Waste Management (LES), Paul Scherer Institut, Villigen PSI, Switzerland, 2014.

[64] K. Salonen, The Selection of Temperature for High Temperature Combustion of Carbon, Acta Hydroch. Hydrob. 7 (1979) 591–597.

[65] E.-M. Köck, M. Kogler, T. Bielz, B. Klötzer, S. Penner, In Situ FT-IR Spectroscopic Study of CO_2 and CO Adsorption on Y_2O_3, ZrO_2, and Yttria-Stabilized ZrO_2, J. Phys. Chem. C. 117 (2013) 17666–17673. doi:10.1021/jp405625x.

[66] T.J. Keskitalo, M.K. Veringa Niemelä, A.O.I. Krause, Modeling of the Adsorption and Desorption of CO_2 on Cu/ZrO_2 and ZrO_2 Catalysts, Langmuir. 23 (2007) 7612–7619. doi:10.1021/la7009868.

[67] N. Huittinen, T. Rabung, A. Schnurr, M. Hakanen, J. Lehto, H. Geckeis, New insight into Cm(III) interaction with kaolinite – Influence of mineral dissolution, Geochim. Cosmochim. Acta. 99 (2012) 100–109. doi:10.1016/j.gca.2012.09.032.

[68] T. Kupcik, T. Rabung, J. Lützenkirchen, N. Finck, H. Geckeis, T. Fanghänel, Macroscopic and spectroscopic investigations on Eu(III) and Cm(III) sorption onto bayerite (β-$Al(OH)_3$) and corundum (α-Al_2O_3), J. Colloid Interf. Sci. 461 (2016) 215–24. doi:10.1016/j.jcis.2015.09.020.

[69] T. Rabung, H. Geckeis, X.K. Wang, J. Rothe, A. Denecke Melissa, R. Klenze, T. Fanghänel, Cm(III) sorption onto γ-Al_2O_3: New insight into sorption mechanisms by time-resolved laser fluorescence spectroscopy and extended X-ray absorption fine structure, Radiochim. Acta. (2006). doi:10.1524/ract.2006.94.9-11.609.

[70] T. Kupcik, Wechselwirkung von dreiwertigen Lanthaniden und Actiniden mit Aluminiumoxiden und -hydroxiden, Inauguraldissertation, University of Heidelberg, 2011.

[71] K.H. Chung, R. Klenze, K.K. Park, P. Paviet-Hartmann, J.I. Kim, A Study of the Surface Sorption Process of Cm(III) on Silica by Time-Resolved Laser Fluorescence Spectroscopy (I), Radiochim. Acta. 82 (1998) 215–219. doi:10.1524/ract.1998.82.special-issue.215.

[72] T. Stumpf, T. Rabung, R. Klenze, H. Geckeis, J.I. Kim, Spectroscopic Study of Cm(III) Sorption onto γ-Alumina, J. Colloid Interf. Sci. 238 (2001) 219–224. doi:10.1006/jcis.2001.7490.

[73] K.T. Jung, A.T. Bell, The effects of synthesis and pretreatment conditions on the bulk structure and surface properties of zirconia, J. Mol. Catal. A: Chem. 163 (2000) 27–42. doi:10.1016/S1381-1169(00)00397-6.

[74] T. Stumpf, T. Fanghänel, A Time-Resolved Laser Fluorescence Spectroscopy (TRLFS) Study of the Interaction of Trivalent Actinides (Cm(III)) with Calcite, J. Colloid Interf. Sci. 249 (2002) 119–122.

[75] T. Kobayashi, T. Sasaki, I. Takagi, H. Moriyama, Solubility of Zirconium(IV) Hydrous Oxides, J. Nucl. Sci. Technol. 44 (2007) 90–94. doi:10.1080/18811248.2007.9711260.

[76] J. Nawrocki, M.P. Rigney, A. McCormick, P.W. Carr, Chemistry of zirconia and its use in chromatography, J. Chromatogr. A. (1993) 229–282. doi:10.1016/0021-9673(93)80284-F.

[77] M. Glorius, H. Moll, G. Bernhard, Complexation of curium(III) with hydroxamic acids investigated by time-resolved laser-induced fluorescence spectroscopy, Polyhedron. 27 (2008) 2113–2118. doi:10.1016/j.poly.2008.04.002.

[78] H. Moll, G. Bernhard, A TRLFS study of curium(III) naphthalene and hydroxyquinoline complexes in aqueous solution, Polyhedron. 31 (2012) 759–766. doi:10.1016/j.poly.2011.11.007.

[79] T. Stumpf, T. Fanghänel, I. Grenthe, Complexation of trivalent actinide and lanthanide ions by glycolic acid: a TRLFS study, J. Chem. Soc., Dalton Trans. (2002) 3799–3804. doi:10.1039/B204679B.

[80] T. Stumpf, A. Bauer, F. Coppin, T. Fanghänel, J.-I. Kim, Inner-sphere, outer-sphere and ternary surface complexes: a TRLFS study of the sorption process of Eu(III) onto smectite and kaolinite, Radiochim. Acta. (2002). doi:10.1524/ract.2002.90.6.345.

[81] M. Marques Fernandes, T. Stumpf, B. Baeyens, C. Walther, M.H. Bradbury, Spectroscopic Identification of Ternary Cm−Carbonate Surface Complexes, Environ. Sci. Technol. 44 (2010) 921–927. doi:10.1021/es902175w.

[82] N. Salem, S. Yakout, Sorption of rare-earth erbium from aqueous solution onto sol-gel-derived zirconia, Hemijska Industrija. 70 (2016) 383–390. doi:10.2298/HEMIND150911040S.